Structural, magnetic and electronic structure studies of $NdFe_{1-x}Ni_xO_3$ ($0 \leq x \leq 0.3$)

2009 J. Phys.: Condens. Matter 21 325501

(http://iopscience.iop.org/0953-8984/21/32/325501)

J. Phys.: Condens. Matter **21** (2009) 325501 (10pp) doi:10.1088/0953-8984/21/32/325501

Structural, magnetic and electronic structure studies of $NdFe_{1-x}Ni_xO_3$ ($0 \leqslant x \leqslant 0.3$)

Abida Bashir[1], M Ikram[1], Ravi Kumar[2], P Thakur[3], K H Chae[3], W K Choi[3] and V R Reddy[4]

[1] Department of Physics, National Institute of Technology, Srinagar 190006, India
[2] Inter University Accelerator Centre, Aruna Asaf Ali Marg, New Delhi 110067, India
[3] Materials Science and Technology Research Division, KIST, Seoul 136-791, Korea
[4] UGC-DAE Consortium for Scientific Research, Khandwa Road, Indore 452017, India

E-mail: abida.nit@gmail.com

Received 24 February 2009, in final form 25 May 2009
Published 20 July 2009
Online at stacks.iop.org/JPhysCM/21/325501

Abstract

We present here the structural, electronic structure, magnetic and Mössbauer studies of $NdFe_{1-x}Ni_xO_3$ ($0 \leqslant x \leqslant 0.3$) samples. All the samples exhibit a single-phase orthorhombic structure with space group $Pbnm$. The near-edge x-ray absorption fine structure (NEXAFS) studies reveal that, with the Ni substitution at Fe sites, a new spectral feature about 1.5 eV lower than the pre-edge structure of $NdFeO_3$ in the O K edge is observed due to the 3d contraction effect and is growing monotonically with the increase of Ni concentration. The Fe $L_{3,2}$, Ni $L_{3,2}$ and Nd $M_{5,4}$ edges confirm the trivalent state of Fe, Ni and Nd ions. The Mössbauer spectra fitted with two Zeeman sextets confirm the different surroundings of Ni around Fe ions. With the increase in Ni concentration, the sextets are broadened. The increase of quadrupole splitting and the decrease of the hyperfine field suggest the change in the ordered regime of the system. The magnetic behaviour at low temperatures is explained in the context of competition among moments of rare earth (Nd) and transition metal ions (Fe/Ni). The strong paramagnetic contribution of the Nd magnetic sublattice and spin flip phenomenon is observed from the temperature dependence of zero-field-cooled and field-cooled magnetization where spin crossover is observed. The isothermal hysteresis loops show a decrease of magnetization and increase of coercivity with the increase in temperature and complements magnetization versus temperature. The results are explained on the basis of the spin reorientation phenomenon.

1. Introduction

Perovskites have been of great interest for many decades because of their relatively simple crystal structure, which displays many diverse electric, magnetic and electronic properties. Oxide perovskites with the general stoichiometry formula ABO_3 have relatively simple structures, which are comprised of corner-linked BO_6 cation-centred octahedra with larger A cations occupying the voids within the three-dimensional framework of the octahedra [1]. The presence of well-defined crystallographic and magnetic sublattices within the same compound, usually leads to very interesting phenomena because of the strong interplay between localized moments, itinerant electrons, magnetic ordering and other important features, which characterize each one of the competing phases. In particular, the rare earth transition metal oxides from the perovskite family are well known due to their striking properties, which are related to exchange mechanisms and the competition between ferromagnetic and antiferromagnetic phases [2].

The studies of the rare earth transition metal oxides have revealed many fascinating aspects. In particular, the doping of homovalent transition metal ions leads to many characteristic changes in the system. In the case of $LaFeO_3$ and $PrFeO_3$, the Ni substitution up to the critical concentration leads to quite unusual properties like the insulator–metal transition, ferromagnetic to paramagnetic transition, etc. The structural, magnetic and electronic studies of Ni-doped $LaFeO_3$ as well

as Ni-doped $PrFeO_3$ have revealed many fascinating aspects concerning the semiconducting ferromagnetic behaviour. The Ni substitution stabilizes the magnetic structure by reducing the asymmetry in hysteresis [3, 4]. These studies on homovalent, Ni^{3+}, substitutions at the iron site reveal the new magnetic behaviour of the ensemble and may cause spin reorientation. The Fe^{3+} and Ni^{3+} states may lead to new magnetic interactions between each other due to the interplay with the intrinsic magnetic behaviour of the rare earth sublattices at low temperatures.

$NdFeO_3$ has an orthorhombically distorted perovskite-type structure and space group *Pbnm*. In $NdFeO_3$, there are three major magnetic interactions: Fe–Fe, Nd–Fe and Nd–Nd [5]. These competing interactions determine their interesting magnetic properties and lead to a number of applications. Mössbauer investigation of the ^{57}Fe-doped nickelates $ANi_{0.98}Fe_{0.02}O_3$ (A = Lu, Y, Tl) have provided independent evidence for the existence of two different Ni sites [6, 7]. The spin reorientation phenomenon has been observed in various Nd–Fe-based compounds including intermetallic compounds such as $Nd_2Fe_{14}B$ [8], $NdDyFe_{14}B$ [9] and $NdFeO_3$ [10–12]. In this paradigm, we have attempted to understand the spin reorientation phenomenon through Ni substitution in the $NdFeO_3$ system, using structural, magnetic and element-specific characterization techniques such as Mössbauer and near-edge x-ray absorption fine structure (NEXAFS) spectroscopy.

2. Experimental details

The polycrystalline bulk samples of chemical composition $NdFe_{1-x}Ni_xO_3$ ($x = 0.0, 0.1, 0.2$ and 0.3), hereafter referred to as NFN0, NFN1, NFN2 and NFN3, respectively, were synthesized by the solid state reaction technique. The stoichiometric amounts of high purity (99.99%) Nd_2O_3, FeO and NiO powders were ground into fine powder in an agate mortar. The mixtures were pressed into pellets and then calcined in air at 1000 °C for 12 h. Calcined samples were sintered twice at subsequently higher temperatures followed by intermediate grinding and pelletization at 1250 °C and 1300 °C for 12 h and 24 h, respectively. To understand the crystal structure, powder x-ray diffraction measurements were performed using a Rigaku Rotaflex x-ray diffractometer with Cu Kα radiation at room temperature (RT) in the 2θ range of 20°–80°. Mössbauer spectra of the samples were recorded using a conventional constant acceleration spectrometer in transmission geometry with a ^{57}Co source in an Rh matrix at RT in the absence of a magnetic field. The Mössbauer spectra were analysed by least-squares fitting using the NORMOS/SITE program developed by Brand[5]. Zero-field-cooled (ZFC) and field-cooled (FC) dc magnetizations as a function of temperature were measured in the presence of a magnetic field of 100 Oe using a PPMS-vibrating sample magnetometer (VSM) from Quantum Design. Isothermal magnetization hysteresis measurements were carried out at different temperatures (10, 200 and 300 K) using the same equipment. The NEXAFS experiments at O K, Fe $L_{3,2}$, Ni $L_{3,2}$ and Nd $M_{5,4}$ edges were performed at the soft x-ray beamline 7B1 XAS KIST of the Pohang Light Source (PLS), operating at 2.5 GeV with a maximum storage current of 200 mA. All the samples were scraped with a diamond file prior to the measurements in order to remove any surface contaminants. All the scans were collected simultaneously in both total electron yield (TEY) and total fluorescence yield (TFY) modes, ensuring both surface (TEY) and bulk (TFY) sensitivities. The close similarity of the spectra taken with these methods verifies that the TEY spectra are representative for the bulk material. The spectra were normalized to incident photon flux and the base pressure of the experimental chamber was better than 1.2×10^{-8} Torr. The energy resolution of the experimental chamber was better than 0.25 eV for L edges of 3d metals.

[5] Laboratorium Für Angewandte Physik, Universität Duisburg, Duisburg, Germany.

Table 1. The lattice parameters and unit cell volumes for different compositions of $NdFe_{1-x}Ni_xO_3$ ($0 \leqslant x \leqslant 0.3$).

Concentration (x)	a (Å)	b (Å)	c (Å)	V^0 (Å^3)
0.0	5.4448	5.5798	7.7523	235.519
0.1	5.4425	5.5738	7.7433	234.543
0.2	5.4377	5.5610	7.7303	233.758
0.3	5.4386	5.5419	7.7292	232.959

3. Results and discussions

3.1. X-ray diffraction

X-ray diffraction studies (XRD) were performed to study the single-phase formation of $NdFe_{1-x}Ni_xO_3$ ($0 \leqslant x \leqslant 0.3$) samples. The XRD data of all the samples were analysed using Rietveld refinement FULLPROF code [13]. Figure 1 shows XRD patterns of $NdFe_{1-x}Ni_xO_3$ (a) $x = 0.1$, (b) $x = 0.2$ and (c) $x = 0.3$ along with the fitted curves and the difference line, which clearly indicates that the XRD patterns are well fitted with space group *Pbnm*. In $NdFe_{1-x}Ni_xO_3$ ($0 \leqslant x \leqslant 0.3$), Nd is associated with Wyckoff position (4c) (x, y, 1/4), Fe/Ni is at position 4b (1/2, 0, 0), O1 is at 4c (x, y, 1/2) and O2 is at 8d (x, y, z). The calculated parameters are shown in table 1. It is clearly evident from table 1 that, with the increase of Ni concentration, the lattice parameters a, b and c decrease and hence their volume also decreases. The decrease in lattice parameters and unit cell volume with Ni substitution confirm that Ni^{3+} has a smaller ionic radii than that of Fe^{3+} and is substituted at the Fe^{3+} site. From the XRD results, the samples with Ni concentrations up to $x = 0.3$ are in single phase having an orthorhombic structure and space group *Pbnm*.

3.2. X-ray absorption spectroscopy

The near-edge x-ray absorption fine structure (NEXAFS) study is most reliable for element-specific characterization, which has been performed to determine the electronic structure and chemical environment of ions (Nd^{3+}, Fe^{3+}, Ni^{3+} and O^{2-}) in the $NdFe_{1-x}Ni_xO_3$ ($0 \leqslant x \leqslant 0.3$) samples. We have collected

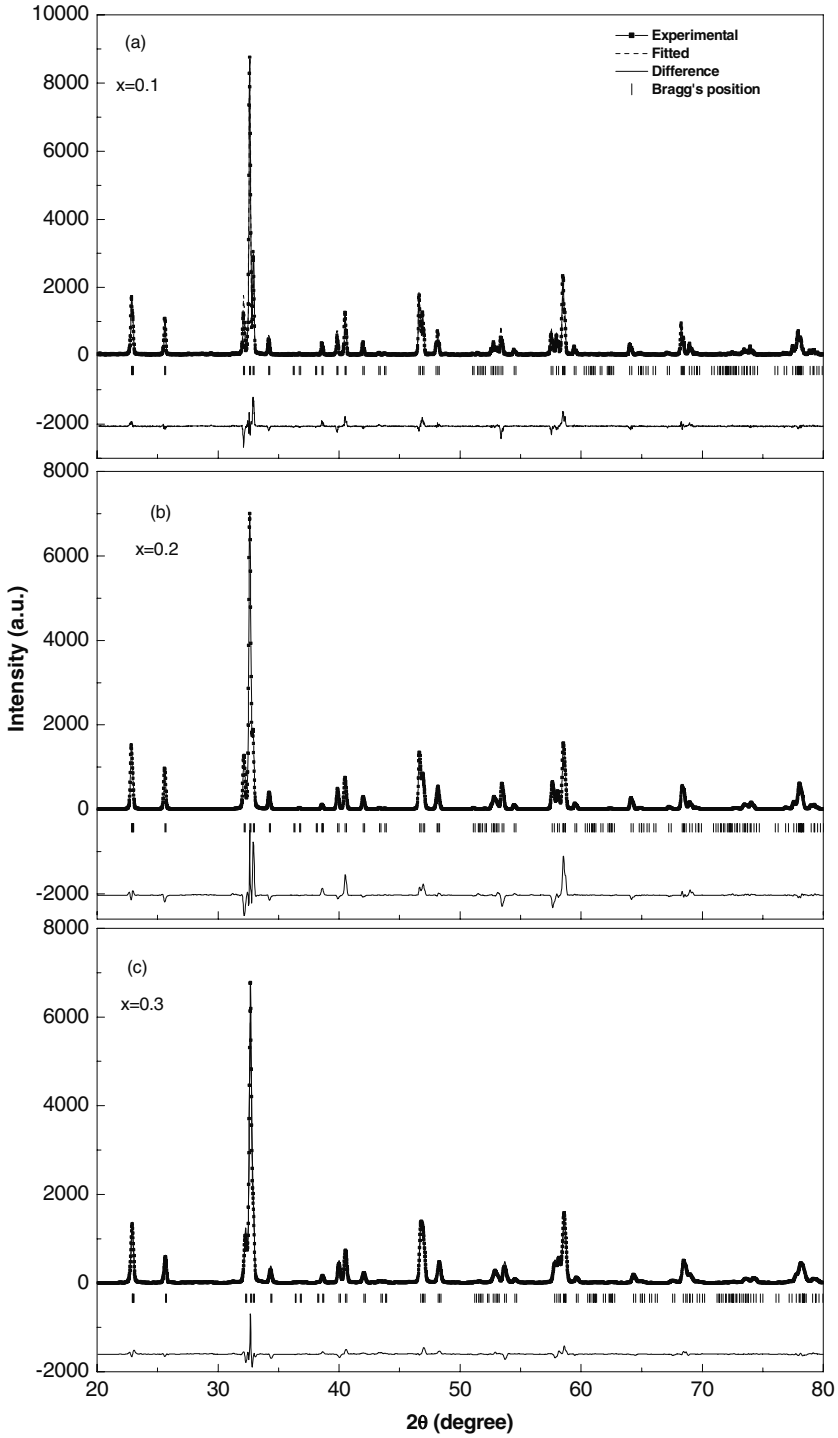

Figure 1. X-ray diffraction pattern of $NdFe_{1-x}Ni_xO_3$ samples for (a) $x = 0.1$, (b) $x = 0.2$ and (c) $x = 0.3$.

the NEXAFS spectra at RT for O K, Fe $L_{3,2}$, Ni $L_{3,2}$ and Nd $M_{5,4}$ edges.

The O K edge probes the unoccupied density of states using dipole selection rules, which arise mainly due to hybridization of O 2p states with 3d states of the neighbouring cations, Fe/Ni, and also the d states of Nd in the present system. de Groot *et al* systematically analysed the pre-peak structure on the O K edge for the series of transition metal oxides [14]. For metal oxides, the structure of the O K edge arises from the covalent mixing of the metal and oxygen states, which introduces O (2p) character into unoccupied states of mainly metal character, making the O (1s) $\rightarrow$ metal (d, s, p) electronic transitions dipole-allowed. The O K-edge spectra of $NdFe_{1-x}Ni_xO_3$ ($0 \leqslant x \leqslant 0.3$) samples collected at RT in TEY mode are shown in figure 2. The O K-edge spectra for the pure compound $NdFeO_3$ may be considered as comprised of doublets labelled as; a, a′ (at ∼528.4 eV and 530 eV), b, b′ (at ∼533.1 eV and 534.4 eV) and c, c′ (at ∼538.8 and 540.8 eV).

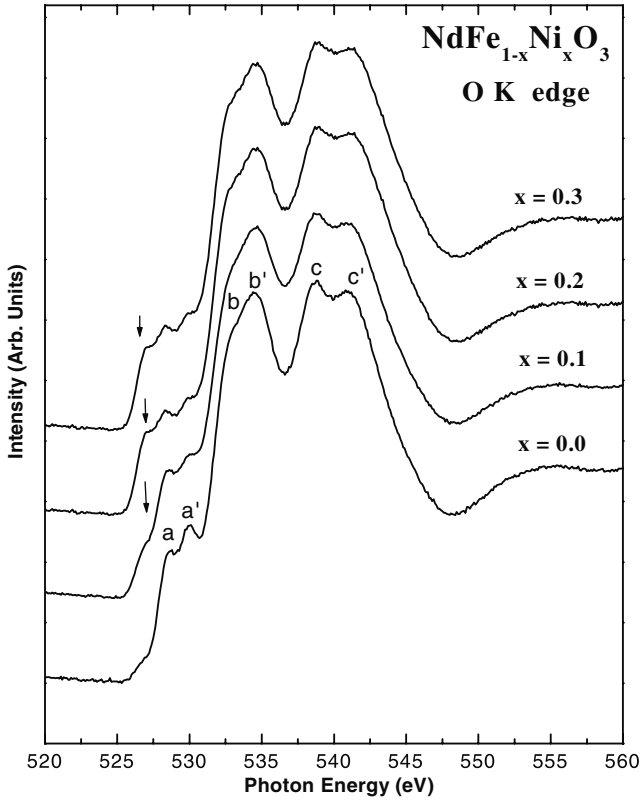

Figure 2. Normalized O K-edge NEXAFS spectra of $NdFe_{1-x}Ni_xO_3$ ($0 \leqslant x \leqslant 0.3$) samples.

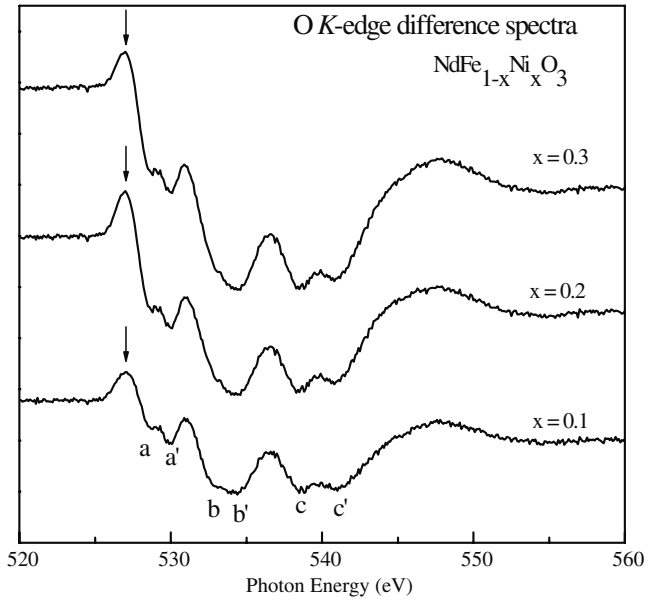

Figure 3. Difference spectra for O K edge (NEXAFS) for $NdFe_{1-x}Ni_xO_3$ ($0 \leqslant x \leqslant 0.3$) samples.

The well-resolved doublets, marked as a and a′ in the spectrum, are related to the transitions from the O 1s to 2p orbitals which are hybridized with Fe 3d orbitals. Moreover, the observed peaks a and a′ are well separated, which corresponds to the crystal field splitting energy 10 Dq $\sim$ 1.4 eV for t_{2g} and e_g orbitals of the Fe 3d levels. Peaks marked as b and b′ (at ∼533.1 and 534.4 eV) can be assigned to the mixed states of O 2p and Nd 3d states, whereas the features in the higher energy region marked as c and c′ are attributed to O 2p hybridization with Fe 4sp/Nd 5sp states and to the scattering resonances at the nearest atoms. All these features observed in the $NdFeO_3$ spectrum are consistent with the earlier reported features in the $PrFeO_3$/$LaFeO_3$ spectrum [3, 4]. With Ni substitution the peaks labelled as b, b′ and c, c′ are getting broader and an additional spectral feature at ∼526.9 eV, approximately 1.5 eV lower than the pre-edge structure of $NdFeO_3$, is observed due to the 3d contraction effect. This pre-edge spectral feature (at ∼526.9 eV) starts dominating with the increase in Ni concentration, because of increasing hybridization between Ni 3d and O 2p orbitals. A similar type of spectral feature has been observed previously by our group in Ni-substituted $PrFeO_3$ and $LaFeO_3$ [3, 4]. Broadening in b, b′ and c, c′ may be attributed to Ni-induced uncertainties in the unoccupied energy levels of higher orbitals (Fe 4sp and Nd 3d/5sp orbitals), which are hybridized with O 2p orbitals. In order to highlight the effect of Ni substitution, the O K-edge spectrum of pure $NdFeO_3$ has been subtracted from the O K-edge spectra for Ni-substituted samples. Figure 3 shows the O K-edge difference spectra, where all the features explained in the O K-edge spectra (figure 2) can be clearly marked but in the form of dips, not as peaks. The increasing dip in the O K-edge difference spectra referring to a decrease of the corresponding peaks observed in the contribution of the pre-edge feature at ∼526.9 eV due to Ni substitution is directly seen. Substitution of the Ni ion effectively causes the increase in the density of states. In the difference spectra increases (i.e. decreases in the unoccupied states), which can be directly observed as increasing dips in all the characteristic peaks from a to c′, are clearer than in the normalized O K-edge spectra (figure 2).

For the description of the 2p XAS spectrum in the case of 3d transition metal compounds, the 3d–3d as well as the 2p–3d two-particle interactions are the most important. These two-particle interactions define the ground state of the transition metal ion splitting the XAS final state into a large number of configurations. Figure 4 shows the normalized NEXAFS spectra of the Fe $L_{3,2}$ edge of $NdFe_{1-x}Ni_xO_3$ ($0 \leqslant x \leqslant 0.3$) samples in TEY mode, which are mainly due to the Fe 2p–3d hybridization and are strongly influenced by the core–hole potentials [15]. These spectra correspond to dipole transitions from Fe $2p_{3/2}$ (L_3) and $2p_{1/2}$ (L_2) core electrons to an unoccupied 3d state ($2p^6 3d^n \rightarrow 2p^5 – 3d^{n+1}$), respectively. Both of these edges further divided into a multiplet structure as a consequence of the interplay of the crystal field and electronic interactions. The observed spectra in the $NdFe_{1-x}Ni_xO_3$ system are similar to the Fe_2O_3 compound reported by Droubay *et al* [16] and Kuiper *et al* [17]. The Fe 2p spectrum can be compared with the $LaFeO_3$ spectrum which exhibits particularly sharp multiplets which have been theoretically simulated assuming a high spin $t_{2g}^3 e_g^2$ ($^6A_{1g}$) ground state with 10 Dq = 1.8 eV, clearly showing that the Fe is in $3d^5$ [18]. Also the Fe 2p spectrum is similar to the equivalent EELS results of α-Fe_2O_3 with Fe^{3+} in octahedral sites [19]. The a_1 and b_1 peaks are due to t_{2g} and e_g orbitals, arising due to the crystal field splitting of the neighbouring ions whose intensity

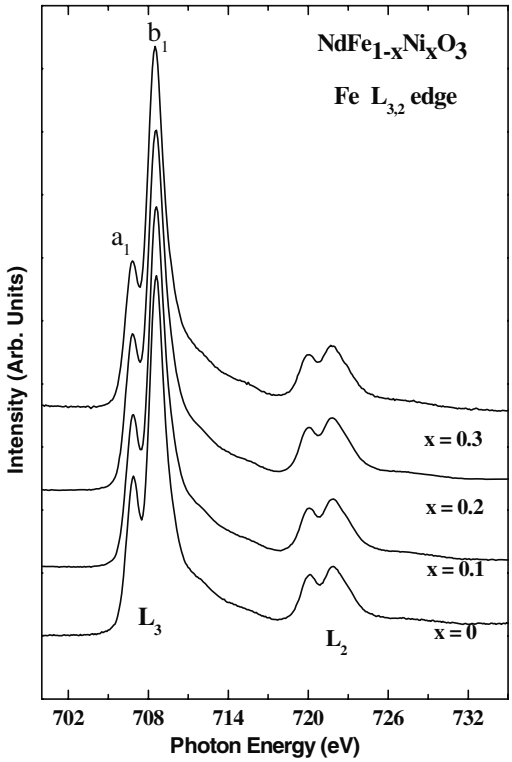

Figure 4. Normalized Fe $L_{3,2}$ edge NEXAFS spectra of $NdFe_{1-x}Ni_xO_3$ ($0 \leqslant x \leqslant 0.3$) samples.

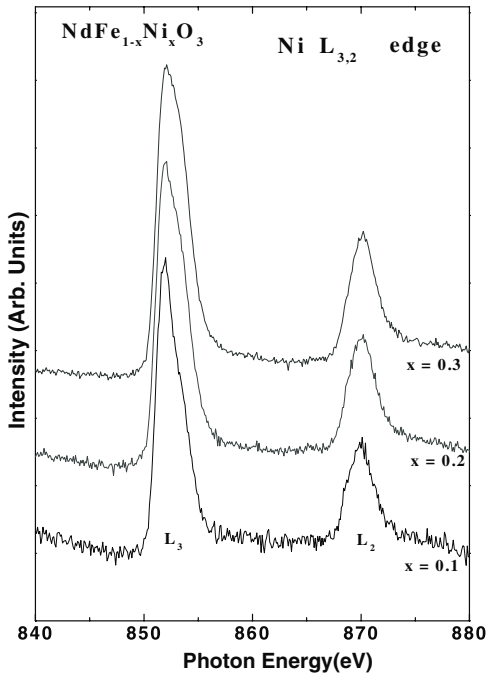

Figure 5. Normalized Ni $L_{3,2}$ edge NEXAFS spectra of $NdFe_{1-x}Ni_xO_3$ ($0 \leqslant x \leqslant 0.3$) samples.

is a direct measure of the total unoccupied states of the Fe 3d states having a crystal field splitting energy of 10 Dq $\sim$ 1.7 eV. Thus, Fe is in the 3+ valence state having octahedral symmetry. Furthermore, there is no change in spectral features nor any shifting of peaks with Ni substitution, indicating that Fe ions remain in the 3+ state for all compositions. The octahedral symmetry of Fe^{3+} ions is also verified from the spectra reported by many groups [3, 4, 15].

Figure 5 shows the NEXAFS spectra at the $L_{3,2}$ edge of Ni collected in TEY mode for the substituted samples only. Similar to the Fe L_3, 2 edge these spectra are in the form of two broad multiplet structures of $2p_{3/2}$ (L_3) and $2p_{1/2}$ (L_2), due to spin–orbit splitting of Ni 2p core holes whose centroids are 18 eV apart. According to the dipole selection rules, Ni 2p electrons can be excited into empty states either with 3d or 4s symmetry. However, the intensity of the 2p to 3d transition is much higher (due to the higher overlap of 3d wavefunctions with 2p orbitals) than 2p to 4s transitions. Therefore, Ni $L_{3,2}$ edge spectra mainly probe the unoccupied states of 3d states. It is well known that spectral feature in the case of the Ni L_3 edge are highly sensitive to the spin states, which decides the unoccupancy in the 3d state [20]. A careful observation shows that the L_3 peak can be deconvoluted into two separate peaks originating due to the t_{2g} and e_g states. The observed spectral features match with the Ni L_3, 2 edge of $PrNiO_3$, where Ni is in the 3+ state having octahedral symmetry [21]. The only difference is that in the $PrNiO_3$ spectra, Ni^{3+} is in a low spin (LS) state, so the doublet due to t_{2g} and e_g at the L_3 edge could be resolved, where unoccupancy in e_g contributes more. Conversely, in our case it is hard to resolve the doublet, the reason being Ni is not in a low spin state but is in a mixed state. This is in agreement with the previous observations [15, 22], and in confirmation of the fact that Ni may have a mixed ground state in octahedral symmetry. There is no change in spectral features and peak positions for systems of higher Ni concentrations which confirms the presence of the Ni^{3+} state in the octahedral environment in these materials.

It is well known that the $M_{5,4}$ spectra offer exact valence-specific information at least for the heavy rare earths because of the localized nature of 4f electrons. In the case of rare earths, intense $M_{5,4}$ resonance spectra are dominated by the spin–orbit splitting of the 3d hole and $3d^{10}4f^n \rightarrow 3d^94f^{n+1}$ transitions, which provide information about the 4f valence state [23]. The comparison with the XAS edges of well-characterized materials can provide information about the valence state of the rare earth in the present compounds. The $M_{5,4}$ edges probe the unoccupied density of Nd 4f states. The absorption edges $3d_{5/2}$ and $3d_{3/2}$, i.e. M_5 and M_4 in the case of Nd are at 978.4 eV and 1000.2 eV, respectively, as has been reported earlier [24, 25], provide clear evidence of the Nd^{3+} state. When the concentration of Ni increases, there is no change in the spectral features of these peaks, giving evidence of the 3+ state of Nd as shown in figure 6. Thus, the XAS studies confirm the chemical state/environment of each ion present in the system and also verify the homovalency of the substituted ions.

3.3. Magnetization studies

3.3.1. Mössbauer studies. Figure 7 shows the Mössbauer spectra of $NdFe_{1-x}Ni_xO_3$ ($0 \leqslant x \leqslant 0.3$) samples at room temperature, in the absence of a magnetic field. The Mössbauer spectra of the ^{57}Fe probe reflect the structural and chemical factors, characterizing not only their local

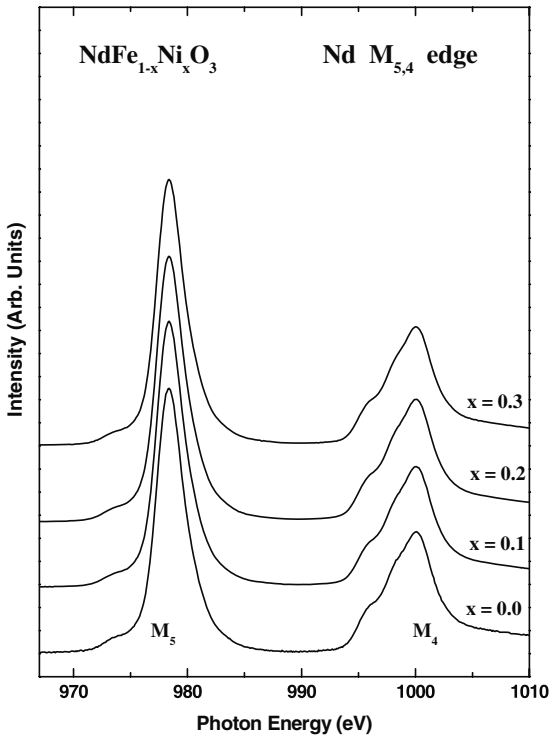

Figure 6. Normalized Nd $M_{5,4}$ edge NEXAFS spectra of $NdFe_{1-x}Ni_xO_3$ ($0 \leqslant x \leqslant 0.3$) samples.

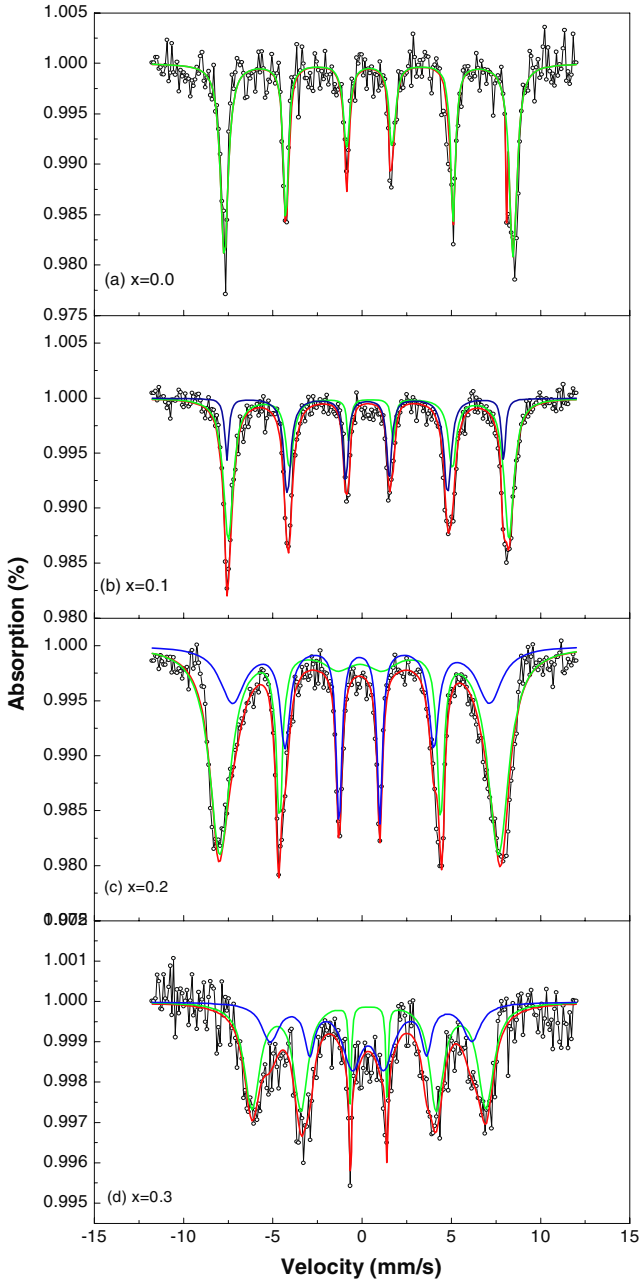

Figure 7. ^{57}Fe Mössbauer spectra of $NdFe_{1-x}Ni_xO_3$ ($x = 0.0, 0.1, 0.2, 0.3$) recorded at room temperature in the absence of magnetic field showing magnetic transitions.

(This figure is in colour only in the electronic version)

environment but also the electronic phenomenon involved in the bulk. Mössbauer studies of rare earth orthoferrites yield a Zeeman-split sextet below the Néel temperature, T_N, and an unsplit line above T_N in agreement with the existence of only one type of crystallographic state of iron [26]. The spectrum of $NdFeO_3$ shows a single sextet (see figure 7(a)) whereas on Ni substitution, for $x = 0.1, 0.2$ and 0.3, two well-defined sextets are observed (see figures 7(b)–(d)). These sextets may be attributed to different distributions of the substituting element. The spectra in the magnetically ordered phase were fitted with sextets associated with Fe nuclei with different local environments. As the concentration of Ni increases, the lines were broadened and the structure of the spectra could not be resolved properly at higher concentrations. Sextet A is having one type of environment of Ni ions surrounded by the Fe octahedra, whereas sextet B is having another type of local environment of Ni ions. The parameters obtained from the Mössbauer spectra are given in table 2. The Fe sublattice is nearly simple cubic, therefore the substitution of Fe by Ni reduces the number of Fe–O–Fe exchange paths. The isomer shift (IS) at the A sextet shows a decrease up to $x = 0.2$, and for $x = 0.3$ it again increases but remains on the lower side from that of pure $NdFeO_3$. For the B sextet, it does show a regular decreasing trend. In general, the isomer shift is negatively proportional to the s-electron density at the nucleus. The decrease in isomer shift is merely indicative of a gradual decrease in volume with increasing Ni concentration. The decrease in volume due to the increase in Ni concentration is also verified from XRD analysis. Taking into account the Fe valence state 3+, the isomer value can be influenced due to the chemical factor, which is the covalency of the Fe^{3+}–O bond, which depends upon the Ni^{3+}–O bond (inductive effect) and a geometric factor corresponding to the Fe^{3+}–O and Ni^{3+}–O bond distances.

The overlap of the Fe inner ns shells ($n = 1$–3) with oxygen $2p_\sigma$ wavefunctions produces a significant change in the s-electron density $\rho_s(0)$ at the iron nucleus. This mechanism is called the overlap distortion effect where the Pauli exclusion principle forces the electrons to keep out of the overlap region to enhance the $\rho_s(0)$ value and thus reduces the isomer shift value. In the case of Ni substitution, the Fe–O distance reduces and the overlap distortion effect plays a role in the decrease of

Table 2. Parameters fitted in Mössbauer spectra of $NdFe_{1-x}Ni_xO_3$ ($0 \leqslant x \leqslant 0.3$).

	IS (mm s^{-1})		QS (mm s^{-1})		Hyperfine field	
Concentration (x)	Sextet A	Sextet B	Sextet A	Sextet B	Sextet A	Sextet B
0.0	0.3900		−0.005 22		50.07	
0.1	0.3563	0.4630	−0.0104	0.308 86	48.67	47.237
0.2	0.3318	0.4150	−0.0894	0.5190	48.23	44.52
0.3	0.3733	0.4044	0.092 73	0.5410	40.45	37.45

the isomer shift value. In addition to the overlap distortion, the decrease is accompanied by an increase of the population of nickel 3d and 4s orbitals, which influences the IS value in the opposite direction [27].

The quadrupole splitting value calculated for the $NdFeO_3$ is almost the same as that of the results obtained earlier, i.e. −0.005 [26]. With the Ni substitution, the quadrupole splitting shows a regular increase in the values for the A as well as the B sextets (see table 2). The hyperfine field arises due to many contributions such as contact, orbital and dipolar contributions. The contact contribution arises from the imbalance of the opposing s-electron density and spin density at the nucleus due to the interaction of the s and unpaired d electrons. The orbital contribution due to a non-zero orbital magnetic moment and the dipolar field depends on the angular distribution of the electrons in the 3d shell and thus on the electric field gradient. The magnetic hyperfine splitting of the spectrum gives a measure of the magnetic moment on the iron atoms and the line intensities enable the orientation of the magnetic moments to be determined. The values of the hyperfine fields at sextet A for NFN1, NFN2 and NFN3 are 48.67, 48.23 and 40.45 T, whereas for sextet B the values are 47.23, 44.52 and 37.45 T, respectively. It is clear that the hyperfine fields show a decrease at the A and B sextets. The lower values of hyperfine fields at sextet A, as compared to the antiferromagnetic rare earth orthoferrites ($H = 54$–56 T), clearly indicates that there is a weakening of interactions between the Fe^{3+} and Ni^{3+} ions which is also clear from the spectrum itself, as the pattern becomes broad and loses its sharp features.

3.3.2. Magnetization. The zero-field-cooled (ZFC) and field-cooled (FC) magnetization as a function of temperature at a 100 Oe field are shown in figures 8(a)–(c) for samples with (a) $x = 0.1$, (b) 0.2 and (c) 0.3. All the samples show irreversible behaviour with closed loops and an intersection of ZFC and FC curves at low temperature regions. The large difference between M_{FC} and M_{ZFC} suggests an inhomogeneous mixture of a ferromagnetic and antiferromagnetic rather than a distinct ferromagnetic or antiferromagnetic long range order. It is evident from figure 8 that the magnetization behaviour indicates the typical canted type antiferromagnetic interactions competing with a ferromagnetic exchange interaction, as has been observed earlier [28–30]. The pure $NdFeO_3$ shows antiferromagnetic behaviour with very low magnetization values in the measured range of temperature (not shown here).

During the FC cycle, magnetization exhibits maxima at temperature T_p. Below T_p, there is a continuous decrease in the magnetic moment. Above T_p with increasing temperature

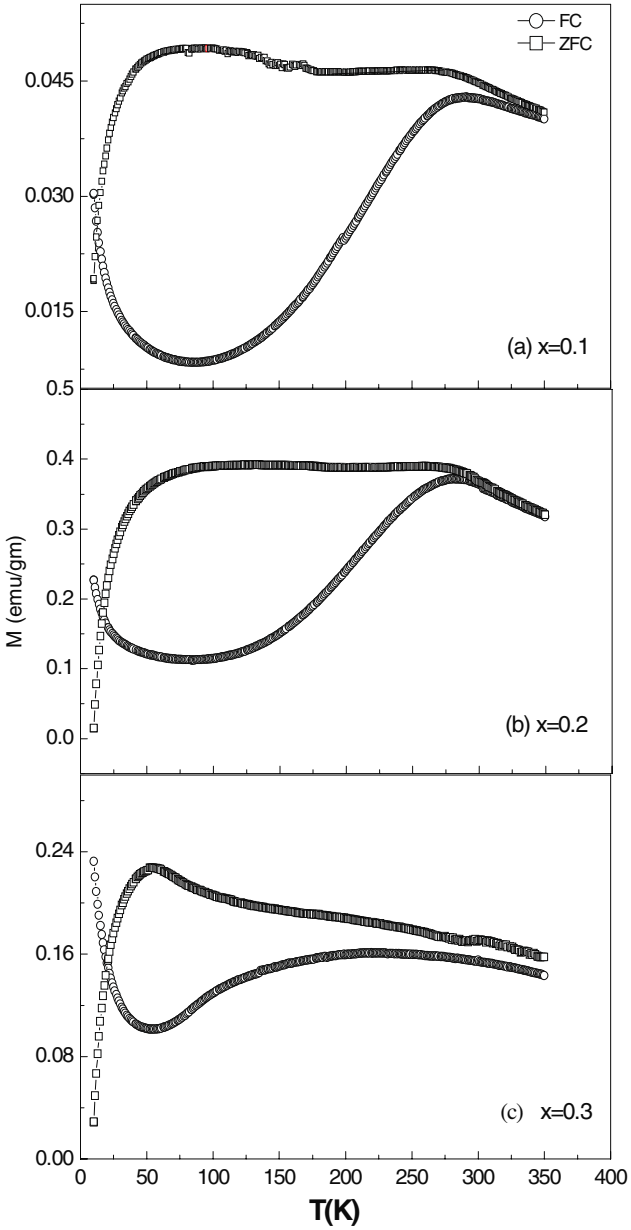

Figure 8. Magnetization versus temperature plots for $NdFe_{1-x}Ni_xO_3$ ($0 \leqslant x \leqslant 0.3$) samples in the presence of 100 Oe magnetic field.

there is the formation of a slight plateau. The plateau features are in the range of 180–265 K and 140–260 K for NFN1 and NFN2, respectively, whereas, in the case of NFN3 there is no plateau seen and magnetization increases with decreasing temperature until it reaches T_p. The plateau resembles the ferromagnetic interactions between the Ni^{3+}

and Fe^{3+} cations. The value of magnetization at T_p for NFN1, NFN2 and NFN3 is 0.045 emu g^{-1}, 0.36 emu g^{-1} and 0.22 emu g^{-1}, respectively. The increase of magnetization in the plateau region clearly indicates the establishment of ferromagnetization between the Fe^{3+} and Ni^{3+} cations up to $x = 0.2$, and with further substitution it is decreased.

A clear crossover between ZFC and FC curves for all the samples was observed at low temperature. The ZFC and FC curves cross each other at considerably lower temperatures. The crossover temperatures (T_{cross}) for the NFN1, NFN2 and NFN3 are 12.96 K, 17 K and 20.61 K, respectively. From this, it follows that the T_{cross} increases with the increase in Ni concentration. The crossover effect is related to the impact of the paramagnetic Nd^{3+} ions, whose magnitude becomes more prominent at lower temperatures. The canted antiferromagnetism of the |Fe + Ni| network and the behaviour of the Nd sublattice contributes independently to the total magnetization. However, during the FC cycle, the ferromagnetically interacting transition metal (Fe/Ni) sublattices will impose a local field over Nd moments. The resultant magnetization hence is the superposition of magnetic moments at both the sublattices (transition metal/rare earth). The inversion of the magnetic moment can be considered as a consequence of the antiferromagnetic exchange interaction between the Nd site and the Fe/Ni sites.

The ZFC/FC curves in the present case can easily be interpreted as a ferromagnetic system with the superposition of two interacting networks; an Fe/Ni-based ferromagnetic sublattice and a negatively polarized Nd sublattice. During the ZFC cycle, the transition metal sublattice, Fe/Ni, behaves as a canted structure. During this process, the Nd moments mainly experience the local field at the Nd sites due to Fe/Ni.

In the mean-field approximation, the magnetization of the Nd moments M_{Nd} will be proportional to the internal field created by the transition metal Fe/Ni moments $M_{|\text{Fe+Ni}|}$. Then the total magnetization M_{tot}, can be written as

$$M_{\text{tot}} = M_{\text{Nd}} + M_{|\text{Fe+Ni}|} = -|J|\chi_{\text{Nd}} M_{|\text{Fe+Ni}|} + M_{|\text{Fe+Ni}|}$$

where we introduced a negative interaction J between the two different sublattices. This expression can be written as

$$M_{\text{tot}} = (1 - \delta\chi_{\text{Nd}}) M_{|\text{Fe+Ni}|}$$

where δ takes into account the strength and sign of the magnetic interaction. According to this relation, at low temperatures the Nd susceptibility, $\chi_{\text{Nd}} \propto 1/T$, becomes sufficiently large; consequently the total moment will reverse its direction.

So, the main important points to explain the inversion of the magnetic moment may be considered as, first, the transition metal sublattices should be in the frozen state below $T = T_{\text{C}}$. Second, the rare earth network should be considered as paramagnetic Nd ions whose magnetization varies as $1/T$. Finally, both the magnetic sublattices should be considered as negatively polarized, i.e. the two interacting networks couple through a negative exchange interaction, i.e. $J < 0$. If the exchange interaction between these two networks becomes negative and, in addition, the magnitude of the rare earth moments is larger than the one due to the ferromagnetic transition metal sublattice, then a ferrimagnetic-like situation with inversion of the spin's direction may occur. Such a type of situation was found in many rare-earth-based solid solutions such as gadolinium- and dysprosium-based solid solutions of manganese oxides [31–33]. In praseodymium–cerium mixed manganites [34], $GdMe_xMn_{1-x}O_3$, where Me is a transition metal atom [35] and the best system to fit this model is $ErCo_xMn_{1-x}O_3$ [36], several magnetic entities coexist, particularly mixed-valence cobalt and manganese ions (Co^{2+}, Co^{3+}, Mn^{3+}, and Mn^{4+}), together with the strong magnetic moment of Er^{3+}.

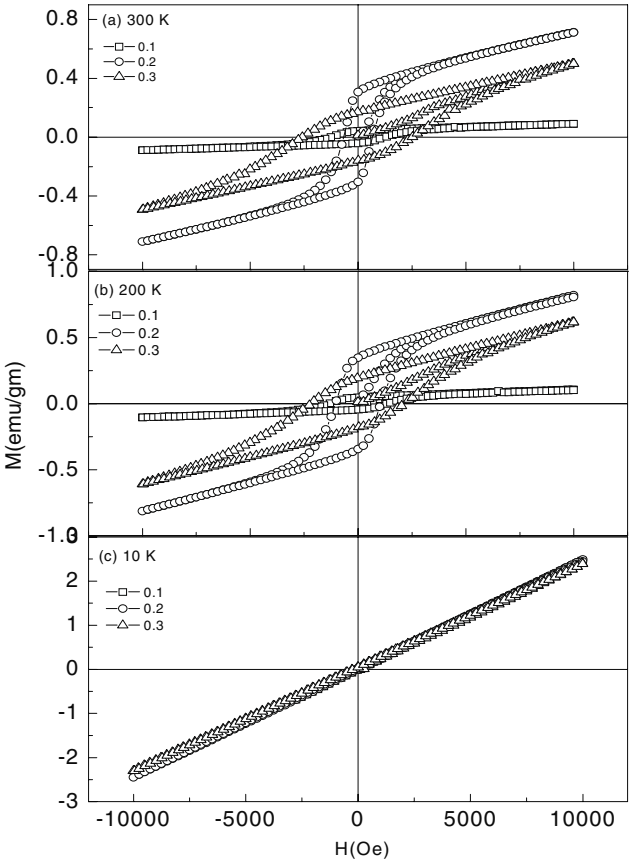

Figure 9. The isothermal M–H loops of $NdFe_{1-x}Ni_xO_3$ ($0 \leqslant x \leqslant 0.3$) samples at (a) 300 K, (b) 200 K and (c) 10 K.

Isothermal magnetization hysteresis measurements were performed at different temperatures (10, 200 and 300 K) for all the samples in order to get an insight about the alignment of the magnetic domains which contribute to the effective magnetic characteristics of the whole ensemble (see figure 9). The parameters extracted from hysteresis curves are given in table 3. At room temperature, i.e. at 300 K, the hysteresis curves are quite pronounced which shows that the coercivity of NFN1 is 1392 Oe and the magnetization M (1 T) = 0.0962 emu g^{-1}, while in the case of NFN2 the coercivity decreases to $H_{\text{C}} = 665$ Oe but the value of magnetization increases to M (1 T) = 0.707 emu g^{-1}. However, the trend changes and the coercivity increases again for the NFN3 system while the magnetization decreases.

Table 3. Parameters extracted from magnetization hysteresis at different temperatures of $NdFe_{1-x}Ni_xO_3$ ($0 \leqslant x \leqslant 0.3$).

Temperature	300 K			200 K		
Concentration (x)	0.1	0.2	0.3	0.1	0.2	0.3
H_C (Oe)	1392.71	664.966	2445.41	1313.65	1054.81	2130.25
M_R (emu g^{-1})	0.043	0.303	0.170	0.048	0.346	0.190
M (1 T)	0.0962	0.715	0.5000	0.102	0.825	0.618

At 200 K, the samples show almost the same behaviour as observed at 300 K, but with a slight increase in the saturation magnetizations. A remarkable change occurs at 10 K, where no hysteresis is observed for any sample and the magnetization shows linear behaviour with magnetic field, indicating that the overall magnetic behaviour is paramagnetic type. The dramatic change in the isothermal magnetization hysteresis loops shows that, at lower temperature, the paramagnetic behaviour of Nd sublattices dominates over the system. Finally, M–H measurements performed at various temperatures between 10 and 300 K complement the magnetization versus temperature data. From the presented magnetization behaviour, we conclude that these materials represent the spin reorientation phenomena. The detailed magnetic structural analysis using neutron diffraction is in progress.

4. Conclusion

Single-phase polycrystalline $NdFe_{1-x}Ni_xO_3$ ($0 \leqslant x \leqslant 0.3$) samples were prepared using the solid state reaction technique. The XRD analysis shows a decrease in volume with the increase in the Ni concentration due to the smaller ionic radii of Ni than Fe. Analysis of the $NdFe_{1-x}Ni_xO_3$ ($0 \leqslant x \leqslant 0.3$) using NEXAFS confirms the octahedral symmetry and oxidation state of the Fe, Ni and Nd ions as 3+. The impact of hybridization increases between the Ni 3d and O 2p orbitals and the very increase of Ni concentration increases the density of states. The Mössbauer spectra revealed that the isomer shift and the hyperfine fields show a decrease along with an increase of quadrupole splitting values with increase in Ni substitution due to overlap distortion. The peak widths are broadened with the increase in Ni concentration and the symmetry is decreased, showing the weakening of the hyperfine field which is evident from the values of the hyperfine field. The temperature-dependent magnetization showed the intersection of the magnetization branches which is intimately connected with the spin reversal phenomenon and the influence of the Nd moments at low temperature. M–H measurements performed at various temperatures show the unsaturated ferromagnetic behaviour at room temperature and coercivity decreases considerably with the decrease of temperature. The dominant paramagnetic contribution of Nd sublattices was clearly supported through M–H measurement. In a nutshell, the doping of Ni at Fe sites enables us to tailor the magnetic properties of the system, showing a transition of magnetic properties, which can be implemented in the applications of magnetic devices and hence controlling the carriers and the moments of these systems.

Acknowledgments

The authors are grateful to Dr Amit Roy, Inter University Accelerator Centre, New Delhi for his keen interest and encouragement to pursue this work. This work was supported by the DST, Government of India under project no. SR/S2/CMP-0051/2007. The Department of Science and Technology (DST), Government of India, is also acknowledged for funding the 14 T-PPMS-VSM at UGC-CSR, Indore.

References

[1] Woodward P M 1997 *Acta Crystallogr.* B **52** 32
[2] Tokura Y 2003 *Phys. Today* **56** 50
[3] Kumar R, Choudhary R J, Khan M W, Srivastava J P, Bao C W, Tsai H M, Chiou J W, Asokan K and Pong W F 2005 *J. Appl. Phys.* **97** 093526
[4] Kumar R, Choudhary R J, Ikram M, Shukla D K, Mollah S, Thakur P, Chae K H, Angadi B and Choi W K 2007 *J. Appl. Phys.* **102** 073707
[5] Bartolome J, Palacios E, Kuzmin M D, Bartolome F, Sosnowska I and Przenios R 1997 *Phys. Rev.* B **55** 1143
[6] Kim S J, Presniakov I A, Demazeau G, Pokholok K V, Baranov A V, Sobolev A V, Pankratov D A and Ovanesyan N S 2002 *J. Solid State Chem.* **168** 126
[7] Kim S J, Demazeau G, Presniakov I A, Pokholok K V, Baranov A V, Sobolev A V, Pankratov D A and Ovanesyan N S 2002 *Phys. Rev.* B **66** 014427
[8] Abache C and Oesterreicher H 1985 *J. Appl. Phys.* **57** 4112
[9] Yelon W B, Foley B, Abache C and Oesterreicher H 1986 *J. Appl. Phys.* **60** 2982
[10] Sosnowska I, Steichele E and Hewat A 1986 *Physica* B **136** 394
[11] Wolf W P 1969 *J. Appl. Phys.* **40** 1061
[12] Karnachev A S, Kovtun N M, Luikina M M and Solovev E E 1977 *Sov. Phys.—Solid State* **9** 950
[13] Carvajal J R 1993 *Physica* B +C **192** 55 2001 Carvajal J R 1993 *IUCR Newslett.* **26** 12
[14] de Groot M F, Grioni M, Fuggle J C, Ghizsen J, Sawatzky G A and Petersen H 1989 *Phys. Rev.* B **40** 5715
[15] van der Laan G and Kirkman I W 1992 *J. Phys.: Condens. Matter* **4** 4189
[16] Droubay T and Chambers S A 2001 *Phys. Rev.* B **64** 205414
[17] Kuiper P, Searle B G, Rudolf P, Tjeng L H and Chen C T 1993 *Phys. Rev. Lett.* **70** 1549
[18] Braun A *et al* 2009 *Appl. Phys. Lett.* **94** 202102
[19] Krivanch O L and Paterson J H 1990 *Ultramicroscopy* **32** 313
[20] Sarma D D, Chainan A, Cimino R, Mathew M and Gudat W 1992 *Europhys. Lett.* **19** 513 Sharma D D *et al* 1994 *Phys. Rev.* B **49** 14238
[21] Medarde M L 1997 *J. Phys.: Condens. Matter* **9** 1679
[22] Piamonteze C *et al* 2005 *Phys. Rev.* B **71** 020406(R)
[23] Kaindl G, Brewer W D, Kalkowski G and Holtzberg F 1983 *Phys. Rev. Lett.* **51** 2056
[24] Thole B T, Laan G V, Fuggle J C, Sawatzky G A, Karnatak R C and Esteva J M 1985 *Phys. Rev.* B **32** 5107
[25] Alexander M, Romberg H, Niicker N, Adelmann P, Fink J, Markert J T, Maple M B, Uchida S, Takagi H, Tokura Y, James A C W P and Murphy D W 1991 *Phys. Rev.* B **43** 333
[26] Eibschutz M, Shtrikman S and Treves D 1967 *Phys. Rev.* **156** 562
[27] Landa B G, de Teresa J M, Ibarra M R, Ritter C, Drost R and Lees M R 1998 *J. Appl. Phys.* **83** 7664

[28] Presniakov I, Demazeau G, Baranov A, Sobolev A and Pokholok K 2005 *Phys. Rev.* B **71** 054409
[29] Hennion M, Moussa F, Carvajal J R, Pinsard L and Revcolevschi A 1997 *Phys. Rev.* B **56** R497
[30] Dabrowski B, Xiong X, Bukowski Z, Dybzinski R, Klamut P W, Siewenie J E, Chmaissem O, Shaffer J, Kimball C W, Jorgensen J D and Short S 1999 *Phys. Rev.* B **60** 7006
[31] de Teresa J M, Ritter C, Ibarra M R, Algarabel P A, Garcia J L, Blasco J, Garcia J and Marquina C 1997 *Phys. Rev.* B **56** 3317
[32] Snyder G J, Booth C H, Bridges F, Hiskes R, di Carolis S, Beasley M R and Geballe T H 1997 *Phys. Rev.* B **55** 6453
[33] Pena O, Bahout M, Ghanimi K, Duran P, Gutierrez D and Moure C 2002 *J. Mater. Chem.* **12** 2480
[34] Pena O, Bahout M, Gutierrez D, Duran P and Moure C 2003 *Solid State Sci.* **5** 1217
[35] Martınez G, Iglesias J R, Ruppenthal A R, Avignon J M and Lacroix C 2001 *J. Magn. Magn. Mater.* **226** 214
[36] Pena O, Ghanimi K, Moure C, Gutierrez D and Duran P 2004 *Bol. Soc. Esp. Ceram. Vidr.* **43** 706